The effect of substrate and surface plasmons on symmetry breaking at the substrate interface of the topological insulator Bi 2 Te 3

SCIENTIFIC REPORTS

OPEN

The effect of substrate and surface plasmons on symmetry breaking at the substrate interface of the topological insulator Bi_2Te_3

Received: 23 August 2018
Accepted: 1 April 2019
Published online: 16 April 2019

Maciej Wiesner[1,2], Richard H. Roberts[2,3], Jung-Fu. Lin[3,4], Deji Akinwande[2,3], Thorsten Hesjedal[5], Liam B. Duffy[5], Shumin Wang[6,7], Yuxin Song[6], Jacek Jenczyk[8], Stefan Jurga[8] & Boguslaw Mroz[1]

A pressing challenge in engineering devices with topological insulators (TIs) is that electron transport is dominated by the bulk conductance, and so dissipationless surface states account for only a small fraction of the conductance. Enhancing the surface-to-volume ratio is a common method to enhance the relative contribution of such states. In thin films with reduced thickness, the confinement results in symmetry-breaking and is critical for the experimental observation of topologically protected surface states. We employ micro-Raman and tip-enhanced Raman spectroscopy to examine three different mechanisms of symmetry breaking in Bi_2Te_3 TI thin films: surface plasmon generation, charge transfer, and application of a periodic strain potential. These mechanisms are facilitated by semiconducting and insulating substrates that modify the electronic and mechanical conditions at the sample surface and alter the long-range interactions between Bi_2Te_3 and the substrate. We confirm the symmetry breaking in Bi_2Te_3 via the emergence of the Raman-forbidden A_{1u}^2 mode. Our results suggest that topological surface states can exist at the Bi_2Te_3/substrate interface, which is in a good agreement with previous theoretical results predicting the tunability of the vertical location of helical surface states in TI/substrate heterostructures.

The Bi_2Te_3 family (Bi_2Te_3, Bi_2Se_3, Sb_2Te_3, and Sb_2Se_3) of topological insulators (TI) was first predicted by Zhang *et al.*[1] to have both topologically protected surface states[2] (TPSS) and an insulating bulk phase[3], which were later confirmed experimentally. In contrast to the three-dimensional TI $Bi_{1-x}Sb_x$, which possesses remarkably complex surface states[4], the surface states of Bi_2Te_3 are much simpler, consisting of only a single Dirac cone[5]. This simplicity makes Bi_2Te_3 an ideal system for studying the physics of TIs. Moreover, with a band gap of 0.17 eV – well above the room temperature energy – Bi_2Te_3 is in principle well-suited for use in electronic devices.

The Bi_2Te_3 family also exhibits tunability of thermoelectric properties[6], phonon dynamics[7], and charge carrier dynamics by adjusting their thickness[8,9]. Importantly, reducing the thickness in a TI increases the surface-to-volume ratio, which significantly enhances the relative contribution of topological surface states to the measured conductance[5,10]. The crystal structure of the Bi_2Te_3 family is characterized by a quintuple layer (QL) structure (Fig. 1a), which is comprised of five atomic, covalently bonded planes, while the QLs are weakly held together van der Waals (vdW) forces. Consequently, Bi_2Te_3 can be mechanically exfoliated similarly to graphene, and thicknesses down to a single QL can be achieved[11]. Upon decreasing the thickness to below 80 nm, the loss of

[1]Faculty of Physics, Adam Mickiewicz University, Umultowska 85, PL61614, Poznan, Poland. [2]Microelectronics Research Center, The University of Texas at Austin, TX78757, Austin, USA. [3]Texas Materials Institute, The University of Texas at Austin, 78757, Austin, TX, USA. [4]Department of Geological Sciences, Jackson School of Geosciences, The University of Texasat Austin, 78712, Austin, TX, USA. [5]Clarendon Laboratory, Department of Physics, Parks Road, University of Oxford, Oxford, OX1 3PU, United Kingdom. [6]Key Laboratory of Terahertz Solid State Technology, Shanghai Institute of Microsystem and Information Technology, Chinese Academy of Sciences, Shanghai, 200050, People's Republic of China. [7]Department of Microtechnology and Nanoscience, Chalmers University of Technology, SE-412 96, Göteborg, Sweden. [8]NanoBioMedical Centre, Adam Mickiewicz University, Umultowska 85, PL 61614, Poznan, Poland. Correspondence and requests for materials should be addressed to M.W. (email: mwiesner@amu.edu.pl)

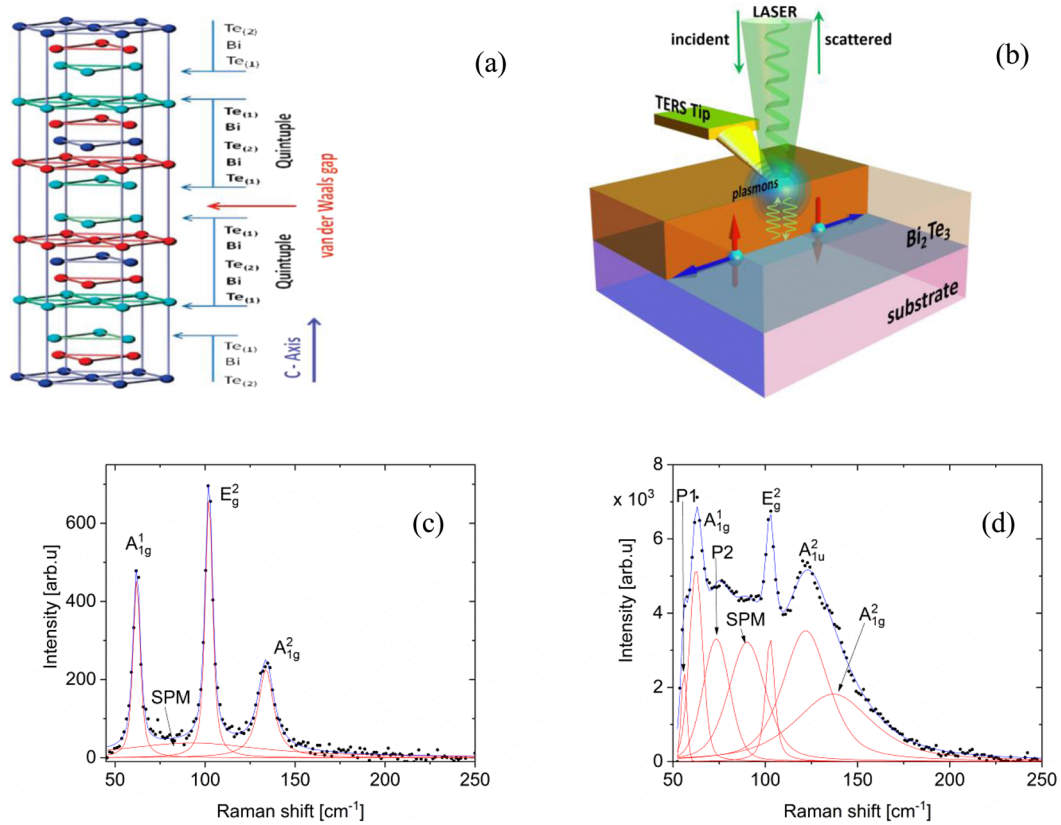

Figure 1. (**a**) Crystal structure of Bi_2Te_3 highlighting quintuple layers (QLs) and the van der Waals gap. (**b**) Illustration of the tip-enhanced Raman spectroscopy (TERS) technique. Characteristic (**c**) micro-Raman and (**d**) TERS spectra of Bi_2Te_3 on a flat sapphire substrate. The A_{1g}^1 and A_{1g}^2 modes are out-of-plane vibrations with respect to the plane of van der Waals-bonded layers, while the E_g^2 mode represents an in-plane vibration. The intensities of the P1 and P2 modes are related to the Bi concentration and the SPM mode to the thickness reduction. The A_{1u}^2 mode is IR-inactive and present in Raman spectra collected from thin TI layers. A detailed description of the modes denoted with red lines is available in the Results section and in the Supplementary Information.

infinite crystal periodicity results in the symmetry breaking along the *z*-axis and consequently in the appearance of the Raman-forbidden A_{1u}^2 mode in Raman spectra of exfoliated Bi_2Te_3[12,13].

Bi_2Te_3 thin films with broken symmetry have been shown to have topologically non-trivial surface states down to ~3 QLs[14].

To date, studies have primarily focused on probing topological surface states at the TI/vacuum interface, which requires careful consideration of surface quality and ultra-high vacuum (UHV) conditions[3]. Studies of the TI/substrate interface, however, may relax the technical requirements as the effect of ambient conditions on the interface quality is negligible[15,16]. Still, atomically smooth TI layers grown via molecular beam epitaxy (MBE) are required for investigations of phenomena taking place at the TI/substrate interface. The quality of the interface and charge carrier properties can then be studied using light scattering spectroscopy[17]. Similarly, surface acoustic phonons have been recently employed as a "sonar" probe of electron-phonon coupling at the interface of Bi_2Te_3 and GaAs[18].

Bi_2Te_3 has a rhombohedral crystal structure with space group D_{3d}^5 ($R\bar{3}m$) and five atoms in the unit cell. From group theory, Bi_2Te_3 has twelve optical branches with the allowed symmetries A_{1g}, A_{2g} E_g, A_{1u}, A_{2u}, and E_u. Since Bi_2Te_3 is centrosymmetric, the rule of mutual exclusion applies: normal modes cannot be both IR and Raman active[13]. However, IR-active modes in the range of ~50–160 cm^{-1} have been observed in Raman[19,20] and inelastic He scattering[21] measurements of Bi_2Te_3. These Raman-forbidden and bulk IR modes arise either from breaking of the crystal symmetry in the *z*-direction (due to the limited thickness of a few QLs) or from surface phonons coupling to topological surface states[13]. At present, the symmetry loss in TI thin films is attributed to a large density of domain boundaries formed during coalescence of crystal islands with different lattice orientations, and the Froehlich electron–phonon interaction has been suggested to play a significant role in the Raman scattering processes[21]. However, Li *et al.* showed that symmetry breaking may also result from the fabrication technique. For example, when using the so-called "scotch tape" exfoliation method, the fragmentation of QLs into sub-quintuple layers leads to the emergence of the Raman-forbidden mode A_{1u} in thick slabs of Bi_2Te_3[14].

In this paper, we present a surface-phonon-based micro-Raman and tip-enhanced Raman spectroscopic (TERS) (Fig. 1b) study of interactions between Bi_2Te_3 and various substrates on which the TI was grown using MBE. Modifications of the interactions are facilitated by the generation of surface plasmons on various substrates, charge transfer from a semiconducting substrate, and a periodic potential applied to the sample via a corrugated sapphire substrate. These interactions induce symmetry breaking in the z-direction of Bi_2Te_3, effectively separating the surface properties from the bulk. Symmetry breaking is manifested in the emergence of Raman-forbidden modes, which imply both modified interactions between Bi_2Te_3 and substrate and modified long-range interactions between Bi_2Te_3 QLs. Our results hint at the possibility of observing topologically protected states at the Bi_2Te_3/substrate interface – even for thick Bi_2Te_3 samples – which would be a breakthrough for fabrication of nanoelectronics devices for lossless electron transport.

Results

Micro-Raman measurements of 50-nm-thick Bi_2Te_3 grown on a flat, insulating sapphire substrate (Fig. 1c) reveal Raman-active A_{1g}^1, A_{1g}^2, and E_g^2 modes in agreement with those previously reported for bulk samples[12] in the range of ~50–160 cm^{-1}. The A_{1g}^1 and A_{1g}^2 modes are out-of-plane vibrations with respect to the plane of van der Waals-bonded layers, while the E_g^2 mode represents an in-plane vibration. The A_{1g} and E_g modes can be used to probe the interactions both between and within QLs. It has been shown that with decreasing Bi_2Te_3 thickness – and consequent decrease in interlayer interactions – the intensity of the A_{1g}^2 mode increases, reflecting less restrained out-of-plane A_{1g}^2 vibrations[22,23]. This decrease in interlayer interaction for thin films also results in the appearance of a surface phonon mode (SPM)[11], which is visible in our micro-Raman spectra at 90 cm^{-1}.

TERS measurements on the same sample (and substrate) show additional excitations that are absent in micro-Raman spectra (Fig. 1d). Two peaks at ~55 and ~76 cm^{-1} (reported in refs[11,24]), labeled P1 and P2, are observed only in TERS spectra. The most striking difference in the TERS spectra is the emergence of the A_{1u}^2 mode at 119.2 cm^{-1}, an IR-active and Raman-forbidden mode that exhibits predominantly out-of-plane atomic motion[25]. Its appearance in Bi_2Te_3 Raman spectra has previously been attributed to symmetry breaking in the z-direction in sufficiently thin films[11]. The observation of this mode in TERS spectra suggests that LSP generation from the TERS technique can also induce symmetry breaking in Bi_2Te_3. LSP generation is evidenced by the more than 10-fold intensity enhancement of TERS spectra compared with micro-Raman spectra[26–28] (see Fig. 1). Further detail on the Raman peaks observed in micro-Raman and TERS measurements of Bi_2Te_3 on sapphire are provided in Table S1.

To confirm that the appearance of the A_{1u}^2 mode is the result of LSP generation and not unique to the sapphire substrate, additional micro-Raman and TERS measurements were performed on 75-nm and 50-nm-thick Bi_2Te_3 grown on semiconducting Si and GaAs substrates, respectively. Figure 2a shows micro-Raman spectra for Bi_2Te_3 on Si, which features the characteristic A_{1g}^1, A_{1g}^2, and E_g^2 modes, as well as a surface phonon mode at ~93 cm^{-1}. The unassigned P2 mode is also present in this sample, along with an additional mode at ~108 cm^{-1} (labeled P3). TERS spectra of the same sample (Fig. 2c) show the emergence of the Raman-forbidden A_{1u}^2 mode, providing further evidence that LSP generation from TERS induces symmetry breaking.

A large signal from the characteristic mode of the Si substrate at ~520 cm^{-1} is observed via TERS measurements, but not in micro-Raman spectra (Fig. S1). Observation of the Si mode suggests that the measurement is quite sensitive to the Bi_2Te_3/Si substrate interface – a result of the difference in the penetration depth for Raman and TERS measurements. The light penetration depth is given by $l = \sqrt{\pi f n \mu_e \mu_m}$, where f is light frequency, μ_e is the electron mobility, μ_m is the magnetic permeability, and n is the electron concentration. We suggest that TERS-induced localized surface plasmons increase the local electron concentration n, leading to an increase of the light penetration depth and consequent appearance of the Si peak.

Micro-Raman spectra of 50-nm-thick Bi_2Te_3 grown on GaAs also exhibit the characteristic Raman-active modes, SPM, and unassigned P2 mode (Fig. 2b). Unlike samples grown on sapphire and Si substrates, however, the Raman-forbidden A_{1u}^2 mode is visible *without* TERS-induced plasmon generation. Consequently, another mechanism must be responsible for symmetry breaking in this sample. As will be further discussed below, a plausible mechanism is charge transfer from the GaAs substrate. TERS spectra on the same sample are nearly identical, but with larger Raman intensities due to the characteristic signal enhancement of the technique (Fig. 2d). Further details of the fittings of Raman spectra for Bi_2Te_3 on Si and GaAs are given in Tables S2 and S3, respectively.

Finally, we examine the effect of a periodic strain potential on 30-nm-thick Bi_2Te_3 films grown on a corrugated sapphire substrate. Due to the instability of sapphire's m-plane surface when annealed at high temperatures, it undergoes spontaneous faceting that results in the formation of V-shaped nanogrooves. Our annealing procedure resulted in substrates with corrugation height and period of $h = 20$ nm and $w = 250$ nm, respectively (Fig. 3a). Bi_2Te_3 was then grown directly onto the corrugated substrate to induce a periodic strain potential. Further details of the procedure are provided in Supporting Information.

Micro-Raman measurements of Bi_2Te_3 grown on corrugated sapphire were carried out with the laser at an incident angle of $\theta = 10°$ with respect to the plane of the substrate (see Fig. 3c). This was done to maintain the same scattering geometry as micro-Raman measurements on flat substrates, compensating for the corrugation angle. For TERS measurements, it is more important that the laser beam is properly focused on the apex of the metallic tip shown in Fig. 1b, rather than on the sample surface, and so the standard angle of $\theta = 0°$ was used. Both micro-Raman and TERS spectra reveal A_{1u}^2 mode emergence (Fig. 3d,e), suggesting that symmetry breaking is induced by the applied periodic strain potential. Additional details of the modes fitted in Fig. 3d,e are listed in Table S4.

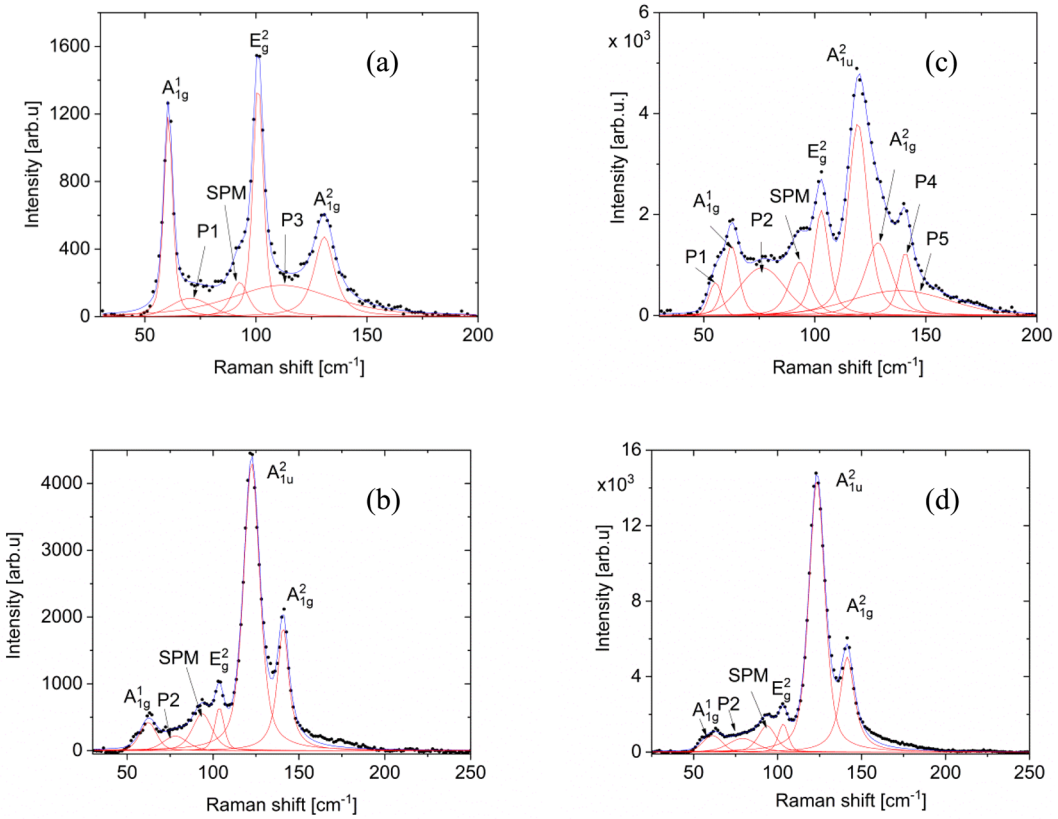

Figure 2. Micro-Raman spectra of Bi_2Te_3 on semiconducting (**a**) Si and (**b**) GaAs substrates; TERS spectra of Bi_2Te_3 on semiconducting (**c**) Si and (**d**) GaAs substrates. Modes P3 and P4 are related to small stoichiometry variations within the area probed by the laser spot. Mode P5 is usually observed only in Raman spectra of 1–2 QL thick layers[11].

Discussion

Broken symmetry of a TI can lead to separation of bulk and surface conduction, and exploiting this phenomenon provides a crucial step forward for experimental studies of TIs and realization of TI-based devices. However, the design process of nanoelectronics devices based on TIs should take into consideration thermodynamic conditions for which the devices are designed. It is a well-known fact that at elevated temperatures, quantum effects are washed out, and, consequently the special properties of the electrically conducting surfaces disappear. Therefore, to suppress the thermal excitation of charge carriers from the bulk into TIs surface states, the energy gap of the system must be increased.

An excellent candidate for nanoelectronic devices is Bi_2Se_3 with a band gap of 0.3 eV, which is twice the value of Bi_2Te_3 of 0.15 eV[1], which makes the observation of TI behavior at room temperature more robust. On the other hand, by decreasing the thickness of Bi_2Te_3 down to 1 QL, its energy gap can reach 0.45 eV[14,29]. This implies suppression of contribution of the bulk electrons into surface states of thin TI layers. Moreover, thermal excitations are related to scattering by acoustic phonons (AP) and decreasing the TI thickness leads to a reduction of bulk AP. Finally, for sufficiently thin TI layers (between 3 QL's and 9 QL's), topologically protected surface states appear[30] and only surface phonons remain. The electron-surface AP coupling[18] can lead to spin-like oscillations of electrons, which can be exploited in device applications. Here, we demonstrated that not only thickness reduction leads to the symmetry breaking, but also LSP generation and interactions of the TI with different substrates. Therefore, we expect that Bi_2Te_3– based devices, grown on selected substrates, will preserve the unique transport properties at the TI/substrate interface even at room temperature. Such conducting edge states at room temperature were recently reported in the two-dimensional TI bismuthene grown on SiC[31].

Previous work has demonstrated that reducing the thickness of Bi_2Te_3 results in symmetry breaking along he z-axis of the material, and consequently the emergence of the Raman-forbidden A_{1u}^2 mode and SPM[11–13,24,32]. Due to the broken symmetry, various surface phenomena have been observed in ultrathin (1-2 nm) Bi_2Te_3[9,12]. Symmetry-breaking in Bi_2Te_3 can also be induced by interactions with the substrate: the effect of a magnetic substrate on symmetry breaking was presented in ref.[33], in which the emergence of ferromagnetism in the bottom surface of Bi_2Se_3 was demonstrated by observation of an additional Shubnikov–de Haas frequency.

In our experiments, we demonstrate three additional mechanisms for symmetry breaking: surface plasmon generation, charge transfer, and the presence of a periodic potential. By employing micro-Raman and TERS spectroscopy, we link the emergence of Raman-forbidden optical phonon modes to underlying broken symmetry of Bi_2Te_3.

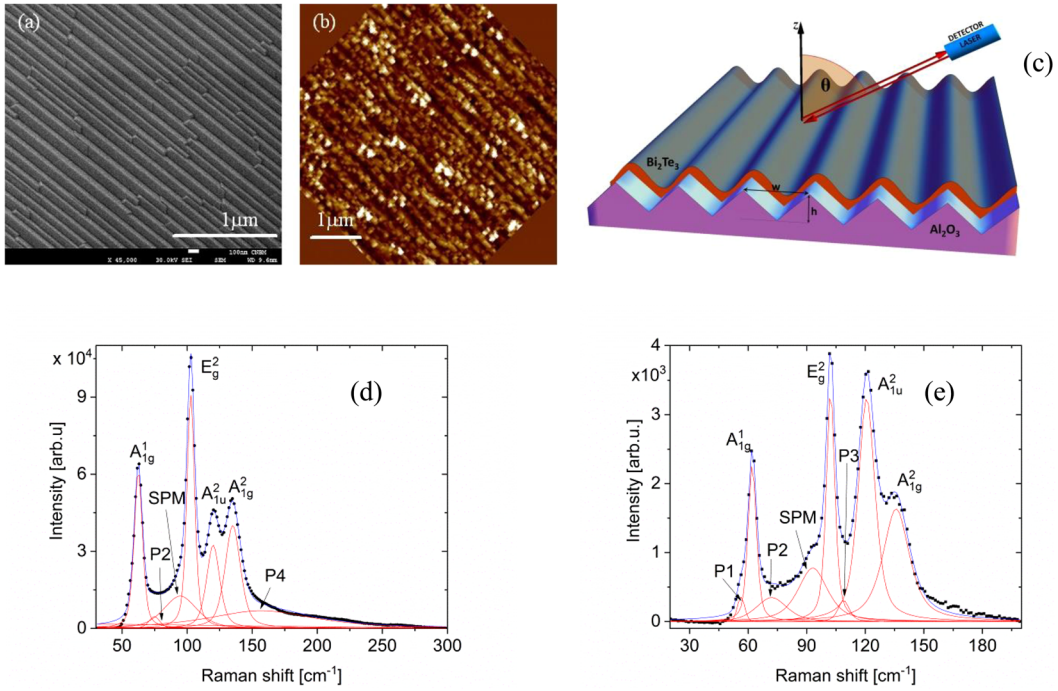

Figure 3. (**a**) Scanning electron micrograph of a sapphire surface with corrugation period $w = 250$ nm and height $h = 20$ nm. (**b**) Atomic force micrograph of a 30-nm-thick Bi_2Te_3 film on the corrugated sapphire substrate. (**c**) Schematic of the experimental geometry for micro-Raman measurements of Bi_2Te_3 grown on a corrugated sapphire substrate with $w = 250$ nm, $h = 20$ nm, and $\theta = 10°$. (**d**) Micro-Raman and (**e**) TERS spectra for a 30-nm-thick Bi_2Te_3 film on corrugated sapphire with the geometry shown in (**c**).

It is well established that the TERS technique uses the local plasmon mode of a sharp metallic nanotip to confine and enhance the electric field near the tip apex. LSP generation in the sample occurs via tip-sample coupling and tip-induced sample heating, which can elevate the sample's temperature[34–36]. The excellent thermoelectric properties of Bi_2Te_3 result in localization of thermally activated electric charges. This, paired with the photoelectric effect from the incident laser light[37–40], results in an increase in local charge density and increases the light penetration depth. We attribute the appearance of the characteristic Raman mode of the Si substrate to this effect, and it is clear evidence of electron-phonon coupling at the Bi_2Te_3/Si interface. A similar effect has been observed with Bi_2Te_3 on a ZnO substrate, for which surface plasmons enhance the photoluminescence from ZnO[41].

Surface plasmons in Bi_2Te_3 can also be generated due to various inter- and intra-band transitions, including bulk interband transitions in the visible range, intraband transitions within topologically protected surface bands in the mid-infrared, and interband transitions between bulk states and topologically protected surface states spanning the UV to near-infrared[35]. The existence of such surface plasmons in Bi_2Te_3 has been confirmed by High Resolution Transmission Microscopy (HRTEM) measurements[28]. In our experiments, LSP generation is evidenced by roughly three- and ten-fold intensity enhancements in TERS measurements compared with micro-Raman for Bi_2Te_3/Si and Bi_2Te_3/flat sapphire samples, respectively. Additionally, LSP generation results in a symmetry breaking of the material evidenced by the appearance of the Raman-forbidden A^2_{1u} mode in TERS spectra.

We also show that electron transfer from the substrate can break the symmetry of Bi_2Te_3, as we observe of the A^2_{1u} mode in both micro-Raman and TERS measurements on a GaAs substrate (Fig. 2). The work functions for GaAs and Bi_2Te_3 are 4.69 eV and 5.3 eV, respectively. Thus, once the materials are in contact, electrons transfer from GaAs to Bi_2Te_3, leading to a large increase in electron density[18,42,43]. The charge transfer from a substrate to a TIis also responsible for tuning vertical location of helical surface states[23]. Wu *et al.* assert that the substantial electronic hybridization at the interface decreases coupling between the first and second QL of the TI, shifting the topologically protected states upward from the first to the second QL.

The A^2_{1u} mode was also observed in both micro-Raman and TERS spectra collected from Bi_2Te_3 on a corrugated sapphire substrate (Fig. 3e). We suggest that the substrate corrugation induces sufficient strain in Bi_2Te_3 to result in symmetry breaking[44]. This agrees with ref.[45], which reports that tensile and compressive deformations of Bi_2Te_3 QLs can cause a shift in the atomic layers of Bi and Te and, as a result, a reduction in symmetry. More detailed theoretical investigations have shown that the lattice constant of Bi_2Te_3 increases at a rate of 0.012 Å per 1% of in-plane uniaxial strain ranging between −6% to 6% (compressive to tensile)[46] and the band gap increased from 0.07 to 0.16 eV between −3 to 3% strain[43]. Strain also induces flexoelectricity and subsequent electric polarization in Bi_2Te_3 – a signature of symmetry breaking in the z-direction[47]. Therefore, uniaxial strain induced by the corrugated substrate can alter the properties of Bi_2Te_3 through both symmetry breaking and strain-induced modifications to the band structure.

Substrate	$I(A_{1g}^2)/I(E_g^2)$	
	micro-Raman	TERS
Si	0.40	0.84
GaAs	2.86	3.39
Sapphire corrugated	0.38	0.49
Sapphire flat	0.34	0.55

Table 1. Ratio of $I(A_{1g}^2)/I(E_g^2)$ for samples investigated with micro-Raman and TERS.

Optical phonons are a common tool for probing intra- and inter-layer interactions between van der Waals-bonded layers such as those in Bi_2Te_3 QLs. Previous studies have demonstrated that the A_{1g}^1 and A_{1g}^2 modes redshift and blueshift, respectively, with decreasing Bi_2Te_3 thickness[11,48] and the intensity ratio $I = \frac{I(A_{1g}^2)}{I(E_g^2)}$ increases with decreasing thickness due to less restrained out-of-plane A_{1g}^2 vibrations[13]. This indicates that the long-range interaction between QLs is weakened as the thickness decreases. The SPM is also a sensitive indicator of Bi_2Te_3 thickness, as it has been shown that the mode increases in intensity as thickness is reduced from 40 nm to a single QL. We observed the SPM mode in all collected micro-Raman and TERS spectra, providing further evidence of weak interactions between QLs in investigated samples. Furthermore, since the out-of-plane and surface modes in Bi_2Te_3 are sensitive to the interaction between QLs, one can use them to derive information about symmetry breaking in the direction perpendicular to the QLs.

Analysis of the intensity ratio I of Bi_2Te_3 on various substrates revealed that local surface plasmon generation, charge transfer, and a periodic strain potential all act to increase I (Table 1). This implies that these mechanisms decrease interlayer interactions in the material – a phenomenon that was previously only associated with thickness reduction in Bi_2Te_3. In each case, the ratio increase is primarily due to an increase in A_{1g}^2 mode intensity rather than a decrease in E_g^2 mode intensity, suggesting that out-of-plane A_{1g}^2 vibrations become less restrained due to weaker interlayer bonding. This effect is most pronounced for the charge transfer mechanism, as I for Bi_2Te_3 on GaAs is nearly an order of magnitude larger than for Si or flat sapphire substrates. For LSP generation and strain mechanisms, the effect is more modest: values of I based on TERS measurements were ~30% larger than those for micro-Raman and ~10% larger for measurements on corrugated compared with flat sapphire. Additionally, the A_{1g}^2 mode was found to blueshift by an average of ~3.5 cm^{-1} in TERS measurements compared with micro-Raman (Tables S1-S4), as would be expected for Bi_2Te_3 exhibiting weaker interlayer bonding.

Based on the emergence of the Raman-forbidden A_{1u}^2 mode and changes in intensities and frequencies of Raman-active optical modes, one can conclude that LSP generation, charge transfer, and application of a periodic potential can each modify the interactions between individual QLs and break the symmetry of bulk Bi_2Te_3. Such effects – which have previously only been observed in Bi_2Te_3 thin films – suggest that isolation of surface phenomena is achievable in bulk Bi_2Te_3 via proper selection of substrate and experimental technique.

Conclusions

The analysis presented herein has shown that LSP generation, charge transfer, and application of a periodic potential can modify the long-range interactions between QLs in a Bi_2Te_3 sample near the substrate interface. This leads to the emergence of Raman-forbidden modes and enhanced out-of-plane vibrations characteristic of topologically insulating Bi_2Te_3 thin films with broken symmetry. Our results highlight the need for further investigations of the quantum Hall effect in Bi_2Te_3 samples with broken symmetry and raise the possibility of isolating topologically protected surface states from bulk states at the interface between Bi_2Te_3 and a substrate – a potential breakthrough for engineering lossless devices based on TIs.

The periodic strain introduced by corrugation causes density fluctuations of the TI layer leading to transverse spin fluctuation[49,50]. For thin TI layers, charge-like and spin-like plasmons can be distinguished, as the first couple to optical and the latter to acoustic phonons, respectively[50]. Investigations of the acoustic phonon dispersion in TIs with and without magnetic field should be able to validate the spin-charge separation hypothesis.

Next, electron transport measurements addressing the Bi_2Te_3/substrate interface should be undertaken to determine if surface conduction can be isolated from bulk via the mechanisms discussed in this work.

Methods

Sample fabrication. Bi_2Te_3 thin films were grown via MBE on Si(111), GaAs (001) with a 2° offcut towards [110], and *m*-plane $[10\bar{1}0]$ cut sapphire (α-Al_2O_3) substrates with flat and corrugated surfaces. The growth temperature was kept at 220 °C. The thicknesses of the Bi_2Te_3 films grown on these substrates were as follows: 75 nm on Si, 50 nm on GaAs, and 30 nm and 50 nm on sapphire substrates. Corrugated sapphire substrates were fabricated using a special heat-treatment procedure that results in surface reconstruction[51–53]. Further details of the sample fabrication are presented in the Supporting Information.

Tip-Enhanced Raman Spectroscopy (TERS) and micro-Raman Spectroscopy. For TERS measurements, a Renishaw inVia spectrometer and NTMDT TERS system were employed in the top-illumination and top-collection type geometry and equipped with a 3 mW, 633-nm wavelength laser.

Micro-Raman spectra were measured in a backscattering configuration using a commercial Renishaw inVia micro-Raman system and a 3 mW, 633 nm wavelength laser. All spectra were measured under 50x magnification resulting in a beam spot about 0.7 μm in diameter. A spectral resolution of about 1 cm^{-1} was achieved using a

1200 l/mm grating. Additional micro-Raman spectra were collected using the NTMD system with a Renishaw spectrometer to compare with TERS measurements; spectra were collected in the tip-retracted position to acquire only the far-field Raman component. The Raman spectra collected using these two systems were comparable.

Details on the TERS technique can be found in the Supporting Information.

Data Availability

Data from Raman and TERS measurements are available upon request to M.Wiesner, mwiesner@amu.edu.pl.

References

1. Zhang, H. *et al*. Topological Insulators in Bi_2Se_3, Bi_2Te_3 and Sb_2Te_3 with a Single Dirac Cone on the Surface. *Nat. Phys.* **5**, 438 (2009).
2. Xia, Y. *et al*. Observation of a Large-Gap Topological-Insulator Class with a Single Dirac Cone on the Surface. *Nat. Phys.* **5**, 398 (2009).
3. Chen, Y. *et al*. Experimental Realization of a Three-Dimensional Topological Insulator, Bi_2Te_3. *Science* **3**, 178 (2009).
4. Hsieh, D. *et al*. Topological Dirac Insulator in a Quantum Spin Hall Phase. *Nature* **452**, 970 (2009).
5. Peng, H. *et al*. Aharonov-Bohm Interference in Topological Insulator Nanoribbons. *Nat. Mat.* **9**, 225 (2010).
6. Guo, M. *et al*. Tuning thermoelectricity in a Bi_2Se_3 topological insulator via varied film thickness. *New J. Phys.* **18**, 015008 (2016).
7. Kim, S. *et al*. Resonance effects in thickness-dependent ultrafast carrier and phonon dynamics of topological insulator Bi_2Se_3. *Nanotechnol.* **27**, 045705 (2016).
8. Li, D. & McGaughey, A. J. H. Phonon dynamics at surfaces and interfaces and its implications in energy transport in nanostructured material. *Nanos. Microsc. Therm.* **19**, 166 (2015).
9. Zhao, J. *et al*. Thickness-dependent carrier and phonon dynamics of topological insulator Bi_2Te_3 thin films. *Optics Express* **25**, 14636 (2017).
10. Xiu, F. *et al*. Manipulating Surface States in Topological Insulator Nanoribbons. *Nat. Nanotechnol.* **6**, 216 (2011).
11. Wang, X. *et al*. *In situ* Raman spectroscopy of topological insulator Bi_2Te_3 films with varying thickness. *Nano Res.* **6**, 688 (2013).
12. Shahil, K. M. F., Hossain, M. Z., Goyal, V. & Balandin, A. A. Micro-Raman spectroscopy of mechanically exfoliated few-quintuple layers of Bi_2Te_3, Bi_2Se_3, and Sb_2Te_3 materials. *J. of Appl. Phys.* **111**, 054305 (2012).
13. Shahil, K. M. F., Hossain, M. Z., Teweldebrhan, D. & Balandin, A. Crystal symmetry breaking in few-quintuple films: Applications in nanometrology of topological insulators. *Appl. Phys. Lett.* **96**, 153103 (2010).
14. Li, Y. Y. *et al*. Intrinsic Topological Insulator Bi_2Te_3 Thin Films on Si and Their Thickness Limit. *Adv. Mater.* **22**, 4002 (2010).
15. Liu, F. *et al*. & micro-Raman, A. study of exfoliated few-layered n-type $Bi_2Te_{2.7}Se_{0.3}$. *Sci. Rep.* **7**, 16535 (2017).
16. Ngabonziza, P. *et al*. *In situ* spectroscopy of intrinsic Bi_2Te_3 topological insulator thin films and impact of extrinsic defects. *Phys. Rev. B* **92**, 035405 (2015).
17. Ruf, T. Phonon Raman Scattering in Semiconductors, Quantum Wells and Superlattices: Basic Results and Applications, *Springer tracts in modern physics*, *Springer-Verlag Berlin Heidelberg New York*. **142**, https://doi.org/10.1007/BFb0110684 (1998).
18. Wiesner, M. *et al*. The electron-phonon interaction at deep Bi_2Te_3-semiconductor interfaces from Brillouin light scattering. *Sci. Rep.* **7**, 16449 (2017).
19. Gnezdilov, V. *et al*. Helical fluctuations in the Raman response of the topological insulator Bi_2Se_3. *Phys. Rev. B.* **84**, 195118 (2011).
20. Kung, H.-H. *et al*. Surface vibrational modes of the topological insulator Bi_2Se_3 observed by Raman spectroscopy. *Phys. Rev. B.* **95**, 245406 (2017).
21. Zhu, X. *et al*. Interaction of Phonons and Dirac Fermions on the Surface of Bi_2Se_3: A Strong Kohn Anomaly. *Phys. Rev. Lett.* **107**, 186102 (2011).
22. Xu, H. *et al*. Raman spectroscopy of epitaxial topological insulator Bi_2Te_3 thin films on GaN substrates. *Modern, Phys. Lett. B.* **29**, 1550075 (2015).
23. Wu, G. *et al*. Tuning the vertical location of helical surface states in topological insulator heterostructures via dual-proximity effects. *Sci. Rep.* **3**, 1233 (2013).
24. He, R. *et al*. Laser induced oxidation and optical properties of stoichiometric and non-stoichiometric Bi_2Te_3 nanoplates. *Nano Res.* **8**, 851 (2014).
25. Cheng, W. & Ren, S. Phonons of single quintuple Bi_2Te_3 and Bi_2Se_3 films and bulk materials. *Phys. Rev. B.* **83**, 094301 (2011).
26. Lu, X. *et al*. Observation and Manipulation of Visible Edge Plasmons in Bi_2Te_3 Nanoplates. *Nano Lett.* **18**, 2879 (2018).
27. Guozhi, J. *et al*. Localized surface plasmon enhanced photothermal conversion in Bi_2Se_3 topological insulator nanoflowers. *Sci. Rep.* **6**, 25884 (2016).
28. Zhao, M. *et al*. Visible Surface Plasmon Modes in Single Bi_2Te_3 Nanoplate. *Nano Lett.* **15**, 8331 (2015).
29. Zhang, Y. *et al*. Crossover of the three-dimensional topological insulator Bi_2Se_3 to the two-dimensional limit *Nat. Phys.* **6**, 584 (2010).
30. Kato, T., Kotaka, H. & Ishii, F. First-principles study of surface states in topological insulators Bi_2Te_3 and Bi_2Se_3: film thickness dependence. *Mol. Simul.* **41**, 10–12 (2015).
31. Reis, F. *et al*. Bismuthene on a SiC substrate: A candidate for a high-temperature quantum spin Hall material. *Science* **357**(6348), 287 (2017).
32. He, R. *et al*. Observation of infrared-active modes in Raman scattering from topological insulator nanoplates. *Nanotechnol.* **23**, 455703 (2012).
33. Buchenau, S. *et al*. Symmetry breaking of the surface mediated quantum Hall effect in Bi_2Se_3 nanoplates using Fe_3O_4 substrates. *2D Mater.* **4**, 015044 (2017).
34. Malkovskiy, V. *et al*. Tip-induced heating in apertureless near-field optics. *J. Raman Spectrosc.* **40**, 1349 (2009).
35. Srinivasan, M. Investigation of thin film thermal transport using micro-Raman thermometry and tip enhanced Raman spectroscopy, http://docs.lib.purdue.edu/open_access_theses.
36. Kemsley, E. K., Potter, J., Belton, P. S., Wilson, R. H. & Marighat, N. A. Effects of sample heating in FT-Raman spectra of biological materials. *Spectrochim. Acta, A* **521571**, 1579 (1996).
37. Zhang, H. *et al*. Anomalous Photoelectric Effect of a Polycrystalline Topological Insulator Film. *Sci. Rep.* **29**, 5876 (2014).
38. Wang, Z., Li, M., Yang, L., Zhang, Z. & Gao, X. P. A. Broadband photovoltaic effect of n-type topological insulator Bi_2Te_3 films on p-type Si substrates, *Nano. Research* **10**, 1872 (2017).
39. Liu, Y. *et al*. Bulk photovoltaic effect at infrared wavelength in strained Bi_2Te_3 films. *APL. Materials* **4**, 126104 (2016).
40. Yin, J. *et al*. Plasmonics of topological insulators at optical frequencies, *NPG Asia. Materials* **9**, 425 (2017).
41. Liao, Z. *et al*. Surface plasmon on topological insulator/dielectric interface enhanced ZnO ultraviolat photoluminescence. *AIP Adv.* **2**, 022105 (2012).
42. Luo, S. *et al*. Significant photoluminescence quenching and charge transfer in the MoS_2/Bi_2Te_3 heterostructure. *J. Phys. Chem. of Solid*, https://doi.org/10.1016/j.jpcs.2017.07.021.
43. Liu, W., Peng, X., Yang, H., Wei, X. & Zhong, J. Fermi level engineering of topological insulator films by tuning the substrates. *J. Phys.: Condens. Matter* **27**, 435003 (2015).
44. Caha, O. *et al*. Growth, Structure, and Electronic Properties of Epitaxial Bismuth Telluride Topological Insulator Films on BaF_2 (111) Substrates. *Cryst. Growth Des.* **13**, 3365 (2013).

45. Zhao, K. *et al*. Strain-engineered atomic-layer movements and valence-band maximum shifts in a two-dimensional single quintuple film of Bi_2Te_3. *Phys. Stat. Sol. B.* **254**, 1600362 (2017).
46. Luo, X., Sullivan, M. B. & Quek, S. Y. First-principles investigations of the atomic, electronic, and thermoelectric properties of equilibrium and strained Bi_2Se_3 and Bi_2Te_3 including van der Waals interactions. *Phys. Rev. B.* **86**, 184111 (2012).
47. Liu, Y. *et al*. Anomalous thermoelectricity in strained Bi_2Te_3 films. *Sci. Rep.* **6**, 32661 (2016).
48. Zhao, Y. *et al*. Interlayer vibrational modes in few-quintuple-layer Bi_2Te_3 and Bi_2Se_3 two-dimensional crystals: Raman spectroscopy and first-principles studies. *Phys. Rev. B.* **90**, 245428 (2014).
49. Raghu, S., Chung, S. B., Qi, X.-L. & Zhang, S.-C. Collective Modes of a Helical Liquid. *Phys. Rev. Lett.* **104**, 116401 (2010).
50. Stauber, T., Gomez-Santos, G. & Brey, L. Plasmonics in Topological Insulators: Spin−Charge Separation, the Influence of the Inversion Layer, and Phonon−Plasmon Coupling. *ACS Photonics* **4**, 2978 (2017).
51. Jenczyk, J., Coy, E. & Jurga, S. Poly(at hylene oxide)-block-polystyrene thin films morphology controlled by drying conditions and substrate topography. *Europ. Polymer J.* **75**, 234 (2016).
52. Park, S. *et al*. Macroscopic 10-terabit-per-square-inch arrays from block copolymers with lateral order. *Science* **323**, 1030 (2009).
53. Gabai, R., Ismach, A. & Joselevich, E. Nanofacat Lithography: A New Bottom-Up Approach to Nanopatterning and Nanofabrication by Soft Replication of Spontaneously Facated Crystal Surfaces. *Adv. Mater.* **19**, 1325 (2007).

Acknowledgements

T.H. acknowledges funding from the John Fell Fund (University of Oxford) and thanks RCaH for their hospitality. L.B.D. acknowledges financial support from EPSRC and STFC (UK). D.A. acknowledges the support of the Lybarger Endowed Faculty Fellowship M.W. acknowledges the support of the Fulbright Senior Award 2016/2017. The paper was partially sponsored by Polish National Centre of Science (NCN) grant 2015/17/B/ST3/02391.

Author Contributions

T.H., L.B.D., S.W. J.J., S.J. and Y.S. grew the samples, M.W., R.H.R., J.-F.L. conducted the Raman and TERS experiments, M.W., D.A. and B.M. analyzed the results, R.H.R., J.-F.L., M.W. and B.M. prepared a draft of the manuscript. All authors reviewed the manuscript.

Additional Information

Supplementary information accompanies this paper at https://doi.org/10.1038/s41598-019-42598-9.

Competing Interests: The authors declare no competing interests.

Publisher's note: Springer Nature remains neutral with regard to jurisdictional claims in published maps and institutional affiliations.